The FASEB Journal article fj.09-141481. Published online October 5, 2009.

ATP modulates Ca^{2+} uptake by TRPV6 and is counteracted by isoform-specific phosphorylation

Dalia Al-Ansary,[*,†] Ivan Bogeski,[†] Barbara M. J. Disteldorf,[†] Ute Becherer,[‡] and Barbara A. Niemeyer[*,†,1]

*Department of Pharmacology and Toxicology, †Department of Biophysics, and ‡Department of Physiology, University of Saarland, Homburg, Germany

ABSTRACT **Ca^{2+} homeostasis requires balanced uptake and extrusion, and dysregulation leads to disease. TRPV6 channels are homeostasis regulators, are upregulated in certain cancers, and show an unusual allele-specific evolution in humans. To understand how Ca^{2+} uptake can be adapted to changes in metabolic status, we investigate regulation of Ca^{2+}-influx by ATP and phosphorylation. We show that ATP binds to TRPV6, reduces whole-cell current increments, and prevents channel rundown with an EC_{50} of 380 μM. By using both biochemical binding studies and patch-clamp analyses of wild-type and mutant channels, we have mapped one relevant site for regulation by ATP to residues within the ankyrin repeat domain (ARD) and identify an additional C-terminal binding region. Stimulation of PKC largely prevented the effects of ATP. This regulation requires $PKC_{\beta II}$ and defined phosphorylation sites within the ARD and the C-terminus. Both regulatory sites act synergistically to constitute a novel mechanism by which ATP stabilizes channel activity and acts as a metabolic switch for Ca^{2+} influx. Decreases in ATP concentration or activation of $PKC_{\beta II}$ disable regulation of the channels by ATP, rendering them more susceptible to inactivation and rundown and preventing Ca^{2+} overload.—Al-Ansary, D., Bogeski, I., Disteldorf, B. M. J., Becherer, U., Niemeyer, B. A. ATP modulates Ca^{2+} uptake by TRPV6 and is counteracted by isoform-specific phosphorylation. *FASEB J.* 24, 000–000 (2010). www.fasebj.org**

Key Words: Ca^{2+} homeostasis · PKC beta II · TRP channels · ATP regulation · allele-specific selection · polymorphism

TRANSCELLULAR Ca^{2+} TRANSPORT is a highly energy-consuming process because Ca^{2+} efflux has to be accomplished against an ~10,000-fold concentration gradient and an ~40–60 mV membrane potential difference. Ca^{2+} influx, in contrast, follows this electrochemical gradient and must be tightly regulated to avoid toxic Ca^{2+} overload. TRPV5 and TRPV6 are highly selective for Ca^{2+}, and their vitamin D-regulated expression in Ca^{2+}-transporting epithelia (*e.g.*, placental tissues and epithelial cells of the intestine and kidney) and in exocrine tissues such as pancreatic acinar and salivary gland cells (TRPV6) make them candidates for selective Ca^{2+} entry (1, 2). In expression systems they are constitutively active at low intracellular Ca^{2+} concentrations (3–5). Ca^{2+}-dependent negative feedback regulation has been studied in detail for both channels (6, 7). TRPV6 shows both a rapid, Ca^{2+}-dependent but calmodulin-independent regulation with involvement of the first intracellular loop (8, 9) and a slower calmodulin-dependent regulation that involves binding of calmodulin to the distal C-terminal region of the protein (10, 11). Depletion of PIP_2 also interferes with Ca^{2+}-dependent inactivation (12) and with permeation block by Mg^{2+}, as shown for TRPV5 (13). But are these the signals that keep channels open if more Ca^{2+} uptake is required? Which regulatory pathways close the channels when sufficient Ca^{2+} has been transferred?

Many ion channels and transporters are regulated by ATP-dependent mechanisms (14–20), but the mechanism and binding sites for Ca^{2+} channels are unknown. For the capsaicin receptor TRPV1 it has recently been shown that binding of ATP within its N-terminal ankyrin repeat domains (ARDs) can prevent capsaicin-induced tachyphylaxis. Here binding of ATP competes with binding of calmodulin (21). Although TRPV6 contains a similar number and a related structure of ARDs as TRPV1, it neither binds calmodulin within its ARDs nor is the ATP binding pocket of TRPV1 conserved (21, 22).

TRPV6 also exhibits a highly unusual coupled polymorphism within the human population (5): although the ancestral allele (TRPV6a: R157, V378, T681) is predominant among African populations, the derived allele (TRPV6b: C157, M378, and M681) is predominant in all other tested population groups, suggesting that this haplotype conferred a temporally or geographically selective advantage (23). The reason for this selection has remained elusive, and no obvious differences in ion channel properties have been found (24). TRPV6 expression correlates with the invasiveness of certain cancers such as prostate cancer and may serve as a prognostic marker for its outcome (25). Whether the

[1] Correspondence: Department of Biophysics, University of Saarland, Kirrberger Str., Geb. 58, 66421 Homburg, Germany. E-mail: barbara.niemeyer@uks.eu

doi: 10.1096/fj.09-141481

increased incidence of prostate cancer among African Americans (26) correlates with the TRPV6 polymorphism is unknown. To understand how channels are regulated by the metabolic status, we investigated the influence and the mechanism of ATP regulation. Because ATP is expected to fuel protein kinases and because the 2 alleles differ in the number of potential PKC phosphorylation sites, we also focused on the regulation by protein kinases.

MATERIALS AND METHODS

Cell culture

HEK293 cells (CRL-1573; American Type Culture Collection, Manassas, VA, USA) and TRPV6 stable cell lines were maintained in a 37°C, 5%CO_2 humidified incubator in Dulbecco's modified Eagle medium (DMEM) containing 10% fetal calf serum and 4 mM L-glutamine and supplemented with 200 U/ml penicillin-G-sodium and 100 μg/ml streptomycin or hygromycin-b (Invitrogen, Carlsbad, CA, USA), respectively. Cells were passaged by treatment with trypsin. Stable cell lines were created from TRPV6a- or -b-expressing vector (pcDNA5/FRT) transfected into Flp-In™-293 cells (Invitrogen) using Superfect Transfection-Reagent (Qiagen, Valencia, CA, USA). Transient transfections of constructs cloned into pCAGGS_IRES_EGFP plasmids were made with Fugene Transfection Reagent (Roche Diagnostics, Mannheim, Germany). Cells were trypsinized and seeded at low density after 24 h and recorded from after ~48 h.

Electrophysiology

TRPV6a (AJ243500) or TRPV6b (AJ243501) stable HEK293 (D11, C3) cells or transiently transfected wild-type or mutant constructs in pCAGGS-IRES-GFP were used for patch-clamp recordings. Recordings were performed at room temperature in the tight-seal whole-cell configuration using electrodes of 2–4 MΩ resistance. Cell capacitance and access resistance were monitored before each voltage ramp, and measurements were discarded when Δ access resistance was >5 MΩ. Series resistance was compensated to 80%. Membrane currents were filtered at 1.5 kHz and digitized at a sampling rate of 5–10 kHz. Currents were recorded with an EPC-9 patch-clamp amplifier controlled by Pulse 8.3 software (HEKA Electronics, Lambrecht/Pfalz, Germany). Immediately after establishing whole-cell configuration, linear voltage ramps from −100 to +100 mV within 100 ms were applied every 10 s from a holding potential of +70 mV for 10 or 20 min as indicated. Currents at −80 mV ramp potential were divided by cell capacitance, normalized (CD/CD_{max}, where CD=current density), and plotted against time. The pipette solution contained the following (in mM): 140 cesium aspartate, 10 EGTA, 10 NaCl, 10 HEPES, and 16 μM $MgCl_2$ or 1 mM $MgCl_2$ with 6 mM Na_2ATP (pH 7.2 with CsOH). The resulting free Mg^{2+} concentration of 11 μM was kept constant for the different concentrations of ATP or other nucleotides by adjusting total [Mg^{2+}] using CaBuf software (ftp://ftp.cc.kuleuven.ac.be/pub/droogmans/cabuf.zip). The bath solution contained the following (in mM): 115 tetraethylammonium chloride, 10 CsCl, 2.8 KCl, 2 $MgCl_2$, 30 $CaCl_2$, 10 glucose, and 20 HEPES (pH 7.4 with NaOH). ATP concentration-response curves were fitted by Eq. 1:

$$Y = \text{base} + \frac{\text{max} - \text{base}}{1 + (X_{1/2}/X)^{\text{rate}}} \quad (1)$$

Statistical analysis was performed using an unpaired, 2-tailed Student's t test. Values of $P < 0.05$ were considered significant.

Fluorescence-based Ca^{2+} imaging

Imaging of free intracellular Ca^{2+} concentration ($[Ca^{2+}]_i$) was performed using an Olympus IX 70 inverted microscope (Olympus Deutschland, Hamburg, Germany) equipped with an ×20 (UApo/ 340, N.A. 0.75) objective, a Polychrome V Monochromator, and a charge-coupled device camera (TILL Imago; TILL Photonics, Gräfelfing, Germany). HEK cells were loaded with 1 μM Fura-2/AM in DMEM growth medium at 37°C for 15 min in a dark chamber. Images were analyzed using TILL Vision software. Bath solutions contained (in mM): 150 NaCl, 2.8 KCl, 1 $MgCl_2$, 1 $CaCl_2$, 20 glucose, and 10 HEPES (pH 7.4 with NaOH) or with 135 NaCl and 10 $CaCl_2$. In the ATP depletion medium NaCl was reduced to 140 mM, glucose was substituted by 20 mM deoxyglucose, and 10 mM sodium azide (NaN_3) was added. The absolute intracellular Ca^{2+}-concentration was calculated as described by Grynkiewicz *et al.* (27).

Fluorescence-based H_2O_2 detection

Intracellular H_2O_2 was detected with the same equipment used for Ca^{2+} imaging. HEK cells were loaded with 1 μM CM-H_2DCFDA [2,7-dichlorofluorescin (DCF); Invitrogen] for 30 min at room temperature. DCF fluorescence was measured at 485 nm excitation and 535 nm emission. GFP fluorescence was used to detect the transiently transfected cells.

Site-directed mutagenesis

Quickchange Site-Directed Mutagenesis Kit (Stratagene, La Jolla, CA, USA) was used to introduce the desired mutations (namely, R153Q/R154P and R606Q) and to mutate the potential phosphorylation sites identified by the prosite software (http://www.expasy.ch/prosite) or the NetPhosK (http://www.cbs.dtu.dk/services/NetPhosK/) by replacing the serine or threonine codons at the specified sites with alanine codons (S144A, T150A, T298A, T299A, S318A, T688A, T702A). The mutated fragments were confirmed by double-stranded sequencing. Unless otherwise noted, mutations were done in the hTRPV6b background.

Cloning and expression of His-tagged proteins

The sequences coding for different fragments of the human TRPV6 N- and C-termini were PCR amplified from hTRPV6b cDNA and subcloned into the *Bam*HI or *Xho*I site of pET19b vector (10 N-term HIS). The fusion protein covering aa 1-117 was made from mouse TRPV6. Protein expression was carried out in transformed *Escherichia coli* BL21 strains. Overnight cultures were diluted 1:20, grown until an OD_{600} of 0.5, and protein production was induced with 100 μM of IPTG for 4 h at 30°C. Cells were pelleted by centrifugation at 6000 *g* for 15 min, and pellets were initially resuspended in 5 mM imidazole, 500 mM NaCl, and 20 mM Tris (pH 7.9). Lysates were sonicated 3 × 30 s and centrifuged at 13,000 *g* for 20 min, and pellets were resuspended in the above buffer with a repeat of sonication and centrifugation. The final resuspension buffer also contained 6 M urea (BBU). Lysates were then incubated with gentle rotation at 4°C for 1 h and pottered with a Dounce homogenizer. Finally, lysates were ultracentrifuged at 24,000 *g* for 25 min at 4°C, and supernatants were incubated

overnight with Ni-NTA beads (Qiagen). Columns were washed once with BBU, then with BBU containing 15 mM imidazole. Proteins were eluted with BBU with 1 M imidazole. The integrity and size of the purified proteins were checked by Coomassie-stained PAGE gels, and protein concentration was determined by BCA (Pierce, Rockford, IL, USA). For native protein expression, ARD (42–266) and CT (633–725) were cloned into a modified pET21b vector (28), and bacteria were induced at an OD_{600} of 0.5 with 75 μM IPTG for 16 h at 25°C. Pellets were resuspended in 20 mM Tris-HCL (pH 8.0), 300 mM NaCl, 20 mM Imidazole, 1 mM PMSF, 0.1% Triton-X-100, 0.2 mg/ml lysozyme, 50 μg/ml RNase, and 25 μg/ml DNase and treated as above. The cleared (20 min at 30,000 *g*) lysates were incubated with Ni-NTA beads for 2 h at 4°C and washed with 20 mM Tris-HCl (pH 8), 300 mM NaCl, and 20 mM imidazole. For elution, imidazole was increased to 200 mM.

ATP-agarose binding

Different His-tagged proteins (40 μg) were diluted to 900 μl with binding buffer: 10 mM Tris (pH 7.5), 50 mM NaCl, 1 mM DTT (no DTT for native proteins), and 0.15% w/v dodecyl-β-D-maltopyranoside (see also ref. 21) with or without 6/15 mM ATP or adenosine, and incubated at 4°C first for 20 min, then with 75 μl of prewashed 50% slurry of ATP-agarose (bound by a C_6-spacer to C-8 of ATP; Sigma-Aldrich, St Louis, MO, USA) for 2 h with gentle rotation. Afterward, beads were sedimented, washed 4 times with 1 ml binding buffer, and resuspended in the corresponding loading buffer, depending on the type of gel and buffer used. Probes were denatured at 37°C for 30 min and separated by 15% SDS-PAGE or 10–20% TRIS/Tricine PAGE. Samples were divided, and gels were either incubated with Coomassie-stain or used to blot the proteins to nitrocellulose or PVDF membranes followed by detection with our own affinity purified antibody against the His-tag. Binding experiments were repeated at least 3 times also with different batches of expressed protein.

RESULTS

ATP prevents rundown of TRPV6 Ca^{2+} currents

To investigate regulation of TRPV6 we recorded either from a stable TRPV6b-expressing cell line that was generated by targeted insertion or from HEK293 cells 48 h after transient transfection. Cells were subjected to voltage ramps at 0.1 Hz for 20 min, and currents were analyzed at −80 mV ramp potential. **Figure 1*A*** shows the development of inwardly rectifying Ca^{2+} currents over time. In the absence of ATP, inward currents reach their maximum within the first 2 min, then decrease continuously to ~30% after 20 min. To quantitate this rundown, we defined the remaining current densities (%REM) at 20 min as percentage of maximum (Fig. 1*B*) and analyzed the time to half-maximal activation ($t_{1/2}$, Fig. 1*C*). Figure 1*D* shows the mean inwardly rectifying current-voltage relationships for TRPV6b at different time points as indicated in Fig. 1*A*. To test whether rundown can be reduced by ATP, we included

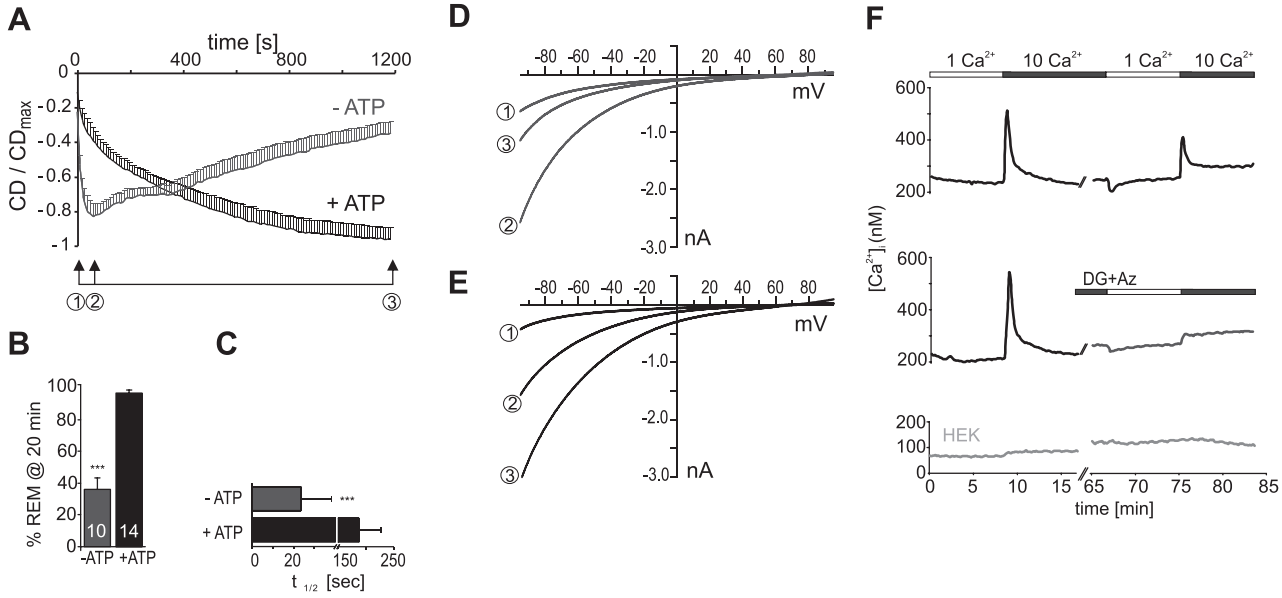

Figure 1. ATP prevents rundown of TRPV6 Ca^{2+} currents. *A*) Whole-cell inward current density (CD) measured from TRPV6b-expressing cells at −80 mV ramp potential normalized to CD_{max} and plotted *vs.* recording time. Traces are averages of normalized CD over time with pipette solution without ATP (gray) or containing 6 mM Na_2ATP (black) and both containing 11 μM free Mg^{2+}. Error bars represent means + SE. *B*) Percentage remaining current (%REM) after 20 min in the absence (gray) and presence (black) of ATP. Numbers on bars represent number of cells. *C*) Quantification of the time to half-maximal activation in the absence and presence of ATP. *D*) Average I/V relationships immediately after break-in (*1*), at 2 min (*2*), and after 20 min (*3*), showing typical inwardly rectifying TRPV6b currents in the absence of ATP. *E*) Sample I/V relationships as described in *D* but in the presence of ATP. *F*) Top panel: Fura-2/AM loaded HEK-TRPV6b cells show a transient increase in Ca^{2+} when extracellular Ca^{2+} is increased to 10 mM. Influx can again be evoked after 1 h if cells are briefly exposed to 1 mM Ca^{2+} bath before the switch. Middle panel: Same protocol as above, but bath solution after the first transient includes 20 mM deoxyglucose instead of glucose and 10 mM sodium azide. Bottom panel: HEK wild-type cells before and after depletion. Traces are averages of > 100 cells for HEK-TRPV6 and 75 cells for HEK wild type.

6 mM Na_2ATP in the recording pipette and clamped $[Mg^{2+}]_i$ to that of the control solution (11 μM). Because $[Mg^{2+}]_i$ is below the IC_{50} for Mg^{2+} block of the pore (29), we can exclude confounding influences on pore properties. Inclusion of ATP led to altered kinetics of current development (Fig. 1*A*): initial current densities were reduced to −16.3 ± 3.4 pA/pF (n=15) compared to −39.7 ± 15 pA/pF (n=11, P>0.5), and subsequent increments in current amplitude were also reduced, leading to current densities that did not decrease within the recording time (Fig. 1*A*), thus resulting in ~100% REM after 20 min (Fig. 1*B*). To test whether the initial reduction in current density was due to an effect of external perfusion of ATP while approaching the cell with the patch pipette, we recorded from cells with no ATP in the patch pipette but locally perfused ATP from a second pipette immediately before and after break-in. However, initial current densities were not reduced (−41.3±6.6 pA/pF, n=4), likely excluding activation of purinergic receptors as the cause of current reduction.

Mean *IV* relationships in the presence of ATP (Fig. 1*E*) indicate that no other major ATP-induced conductances were observed with our recording conditions but revealed a minor decrease in the steepness of inward rectification. A shift in the same direction is seen in the absence of ATP when EGTA is replaced by BAPTA (data not shown), which may indicate a decrease in the Ca^{2+}-dependent feedback mechanism when adding ATP to the EGTA pipette solution. To exclude the possibility that ATP is preventing rundown solely by increasing the fast calcium-buffering capacity of the pipette solution, we confirmed that ATP still had significant effects in the presence of 20 mM BAPTA (data not shown). Prevention of rundown by ATP has also been shown in Ca^{2+}-free conditions (30). The maximal current densities for TRPV6b after 20 min with ATP were −153 ± 11 pA/pF, which were not different when compared to the maximal current densities without ATP (−160±27 pA/pF).

The effects of ATP on both kinetics of current development and on rundown were also seen with transient expression of TRPV6b. Rundown and $t_{1/2}$ were analyzed at 10 min recording time, as transiently expressing cells were less stable. Whereas in the absence of ATP the kinetics of current development, maximal current density, and the degree of rundown were comparable for transient *vs.* stable transfected cells (Supplemental Fig. S1*A*), in the presence of ATP the slowdown of current development was also significant, but less pronounced than with stable TRPV6 expression ($t_{1/2}$ 57±10 *vs.* 117±22 s for transient and stable expressed TRPV6b, respectively; Supplemental Fig. S1*A, B*). Because oxidation has been shown to modulate binding of ATP to chloride channels (31), we used the fluorescent indicator DCF to test whether transient expression influences the redox state of the cells. Indeed, Supplemental Fig. S1*C* shows that transiently transfected cells showed higher levels of intracellular oxidants than stable cells. We thus investigated the influence of oxidants (H_2O_2) on the time course of TRPV6 in the stable expression system. Supplemental Fig. S1*D* shows that increasing oxidative stress through addition of H_2O_2, probably by modifying reactive cysteines of TRPV6, leads to larger current increments in the presence of ATP and can thus explain the faster current development in cells transiently expressing TRPV6. However, even in the presence of a strong oxidant, ATP is still able to prevent rundown (Supplemental Fig. S1*D*). For further analyses, we have focused on the effects of ATP on the percentage of rundown (%REM) and compared rundown at 20 min for stable and at 10 min for transient expression.

To mimic a more physiological condition, we tested the influence of ATP depletion (32) on Ca^{2+} transients in unperturbed cells. Figure 1*F* shows that TRPV6 cells respond to a change in $[Ca^{2+}]_e$ with a transient increase in $[Ca^{2+}]_i$. This transient increase can again be evoked after ~50 min (Fig. 1*F*, top panel). However, when TRPV6 cells are ATP depleted, the second transient peak is absent (Fig. 1*F*, middle panel), confirming that either a sufficient concentration of ATP or of a metabolite is needed for the ability to respond to sudden changes in $[Ca^{2+}]_e$. HEK cells show a lower resting Ca^{2+} and do not show a transient increase in $[Ca^{2+}]_i$ on exposure to 10 mM $[Ca^{2+}]_e$ (Fig. 1*F*, bottom panel). Interestingly, in HEK cells, the change back to 1 mM $[Ca^{2+}]_e$ does not lead to a drop in $[Ca^{2+}]_i$ (Fig. 1*F*, top panel), which may be due to Ca^{2+}-ATPase inactivity at low resting $[Ca^{2+}]_i$ (K_m 0.4–0.5 μM; 33).

Thyagarajan *et al.* (12) showed that hydrolysis of PIP_2 mediated Ca^{2+}-induced inactivation of TRPV6 channels (12). To test the potential involvement of PIP_2 in the ATP effect, we replaced ATP with 50 μM diC_8PIP_2, which was unable to prevent rundown in the absence of ATP (**Fig. 2*A*, *B***). We also included a nonhydrolyzable ATP analog, AMP-PCP, in the pipette solution. This analog also prevented rundown and slowed current development (Fig. 2*A, B*). Because R599 was identified as a critical residue responsible for mediating PIP_2-dependent channel activity in TRPV5 (34), we checked whether this highly conserved arginine mediates the ATP effect in TRPV6 (R599 in rbTRPV5=R606 in hTRPV6). We mutated R606 to Q and recorded the transiently expressed mutant in the presence and absence of ATP. Figure 2*C, D* shows that ATP is still able to prevent rundown in the mutant. Together with the evidence seen in Fig. 2*A*, the results suggest that ATP prevents rundown of TRPV6 in a PIP_2-independent manner.

Nucleotide specificity

To further test the specificity of the ATP effect, we included different nucleotides in the pipette solution at 6 mM each. **Figure 3*A*** shows currents over time for some of the tested nucleotides, and Fig. 3*B* the percentage REM for all nucleotides tested. Although adenosine and cAMP were unable to prevent rundown, other phosphorylated nucleotides had intermediate effects,

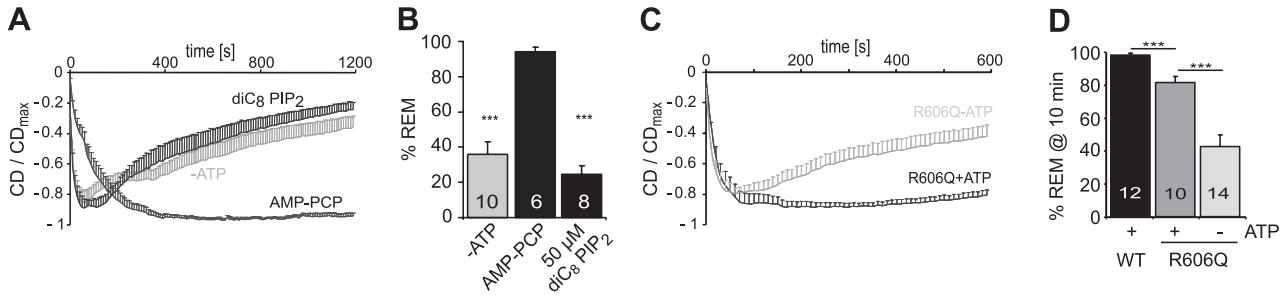

Figure 2. Effects of PIP_2 and a nonhydrolyzable ATP analog on rundown. *A*) Normalized current density over time in the absence of ATP (gray trace), in the presence of 50 μM diC_8PIP_2, or in the presence of 6 mM AMP-PCP in TRPV6b stable cell line. *B*) Percentage REM for traces in *A*. *C*) R606Q mutants retain the ATP effect. Normalized current density over time for transiently expressed TRPV6_R606Q mutants with and without ATP in the recording pipette. *D*) Percentage REM after 10 min recording time; see also Fig. 5*B* for transiently expressed wild type.

with AMP being more potent than GTP and slightly more potent than UTP, which suggests that both nucleotide moiety and number of negatively charged phosphate groups are essential (Fig. 3*A*). To test the dependence of rundown on the ATP concentration, we calculated the dose response relationship after recording currents with different free ATP concentrations, keeping free [Mg^{2+}] constant. Figure 3*C* shows sample traces of currents with 6, 304, and 609 μM and 3.7 mM free ATP in the pipette solution. Data points were fitted with a sigmoidal dose-response function of variable slope, where $\%REM_{max}$ is the maximal remaining current obtained after addition of 3.7 mM free ATP, EC_{50} is the half-maximal concentration of free ATP, and n is the Hill slope. As shown in Fig. 3*D*, the mean EC_{50} obtained from the graph was 378 μM free ATP, and the Hill slope was 4.8. The EC_{50} value obtained is one order of magnitude greater than that normally required for a kinase-mediated phosphorylation reaction (14); however, we also investigated the crosstalk between rundown and PKC-mediated phosphorylation.

Regulation by protein kinase C and identification of a functionally relevant ATP binding site

To measure TRPV6 currents in the presence of ATP and after activation of protein kinases, we incubated cells for 1 h with 500 nM PMA in serum-free medium and then recorded with PMA also present in the bath solution. **Figure 4*A*** shows that incubation with PMA was able to partially prevent the effects of ATP: Although ATP was included, current size increased much faster, reached maximal values within the first 2 min, and entered rundown (Fig. 4*A*, *B*).

Because the ancestral polymorphic allele (TRPV6a) contains an additional potential PKC phosphorylation site (SPR^{157}) compared to SPC for TRPV6b, we also tested the effects of PMA treatment on TRPV6a and found a slightly more efficient prevention of the ATP effect (Fig. 4*C*, *D*). In the absence of ATP, PMA treatment had little effect on rundown (Supplemental Fig. S2*A*, *B*). The finding that the polymorphs differ slightly in the extent of the PMA effect may point

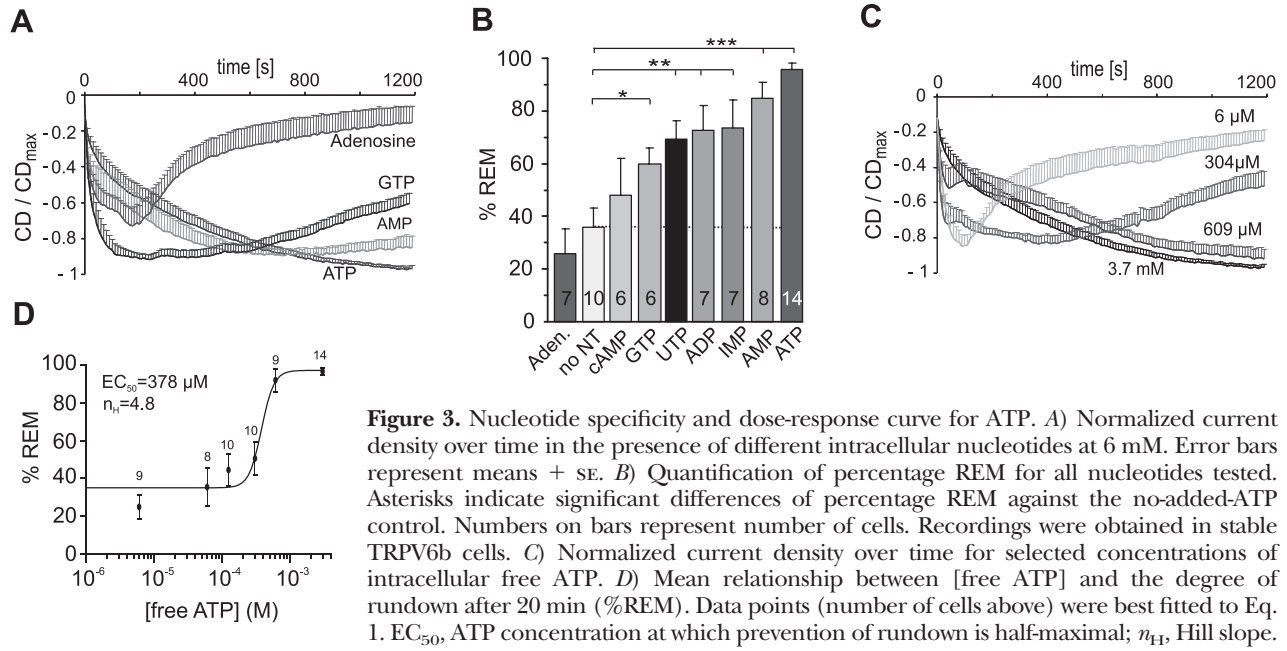

Figure 3. Nucleotide specificity and dose-response curve for ATP. *A*) Normalized current density over time in the presence of different intracellular nucleotides at 6 mM. Error bars represent means + SE. *B*) Quantification of percentage REM for all nucleotides tested. Asterisks indicate significant differences of percentage REM against the no-added-ATP control. Numbers on bars represent number of cells. Recordings were obtained in stable TRPV6b cells. *C*) Normalized current density over time for selected concentrations of intracellular free ATP. *D*) Mean relationship between [free ATP] and the degree of rundown after 20 min (%REM). Data points (number of cells above) were best fitted to Eq. 1. EC_{50}, ATP concentration at which prevention of rundown is half-maximal; n_H, Hill slope.

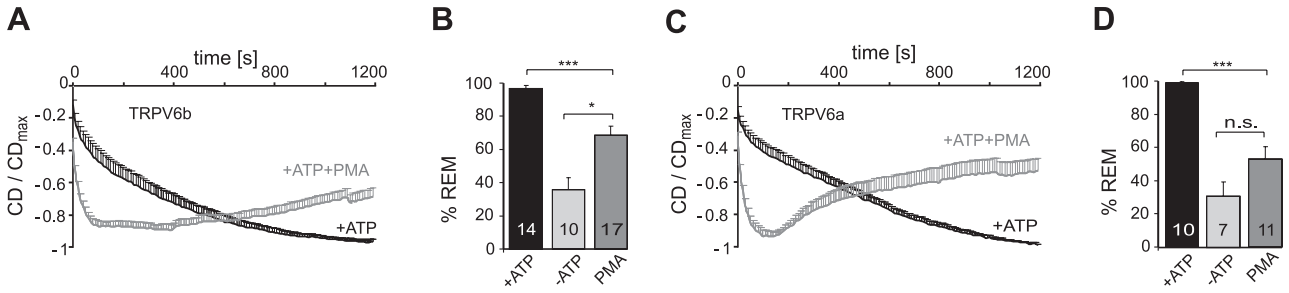

Figure 4. Stimulation of PKC counteracts ATP-dependent stabilization of currents. *A*) Normalized current density over time for TRPV6b-expressing control cells (black trace) and cells that were pretreated for 1 h with 500 nM PMA (dark gray trace). *B*) Quantification of rundown (%REM) after 20 min for recordings in *A*. *C, D*) Normalized current densities over time (*C*) and quantification of %REM (*D*) as described in *A, B* for TRPV6a-expressing cells.

toward S155 being involved in preventing the ATP effect. S155, as well as the joint first putative phosphorylation site S144, is located within the ARD in a loop between repeats 3 and 4 (see ref. 22 for structural information). We wondered whether phosphorylation can partially suppress the effects of ATP because of the charge screening effect of the phosphorylated (negative) moiety onto nearby positively charged side groups required for a direct interaction with the phosphate groups of ATP. If this were so, one would predict that this region also would contain residues important for ATP binding. Two positively charged arginine residues (R153/R154) are in proximity to the S144 phosphorylation site and adjacent to the polymorphic phosphorylation site S155 (**Fig. 5*A***). We thus mutated these residues (RR/QP) and recorded currents in the presence of 3.7 mM free ATP. As seen in Fig. 5*B, D*, ATP was now unable to prevent fast activation and rundown, confirming a functional importance of R153/R154. In addition, initial current densities [−29.8 pA/pF (−ATP) *vs.* −29.4 pA/pF (+ATP)] were identical, and maximal current densities were slightly larger than wild type. Reversion of the positive charges by mutating arginine into glutamate (RR/EE) resulted in an ~90% reduction in both initial and maximal current sizes, demonstrating that negative charges in this position critically affect ion channel function. Charge reversion also partially mimicked the current stabilizing effect of ATP by reducing the percentage REM in the absence of ATP to 70.5 compared to 45 for wild type ($P<0.5$). To further test that this region contains a functionally relevant ATP binding site, we included a peptide containing the sequence from aa 147 to 165 (see Fig. 5*A*) together with ATP in the patch pipette. Figure 5*C, E* shows that the peptide was indeed able to compete with ATP and induce rundown. To test for direct binding of ATP to this protein region, we expressed and purified the protein fragment covering the ARD of wild-type and RR/QP mutants and tested their ability to be retained by ATP-agarose. Wild-type ARD is retained by ATP-agarose,

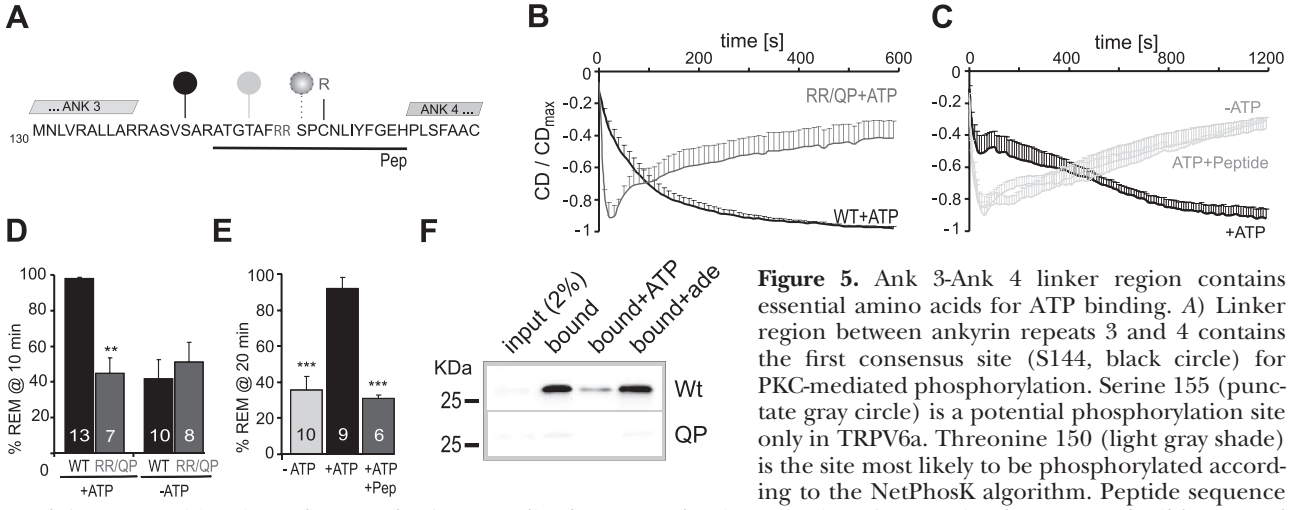

Figure 5. Ank 3-Ank 4 linker region contains essential amino acids for ATP binding. *A*) Linker region between ankyrin repeats 3 and 4 contains the first consensus site (S144, black circle) for PKC-mediated phosphorylation. Serine 155 (punctate gray circle) is a potential phosphorylation site only in TRPV6a. Threonine 150 (light gray shade) is the site most likely to be phosphorylated according to the NetPhosK algorithm. Peptide sequence used for competition is underscored. *B*) Normalized current density over time for transiently expressed wild-type and R153Q/R154P mutants in the presence of 3.7 mM free ATP. *C*) Normalized current density over time for stable TRPV6b-expressing cells recorded in the presence of 609 μM free ATP (black trace), 609 μM free ATP + 2 mM competing peptide encompassing sequence underscored in *A* (dark gray trace), or without added ATP (light gray trace). *D, E*) Quantification of rundown at 10 min for transient cells (*D*) and at 20 min for stable cells (*E*). *F*) ATP-agarose pulldown experiment with wild-type or RR/QP mutant fusion protein of the ARD (aa 42–266). Input (2% of total) or bound His-tagged fusion proteins were detected by Western blot using an anti-HIS antibody. Binding was competed with 6 mM ATP but not with 6 mM adenosine (ade).

and binding can be competed for by free ATP or UTP (data not shown), but not by adenosine (Fig. 5*F*). In contrast, RR/QP-ARD showed a significant reduction in binding to ATP-agarose (Fig. 5*F*). Together, these results suggest that the ARD 3–4 region with residues R153/154 mediate binding of ATP's negatively charged moieties and is responsible for its physiological effects. Phosphorylation at S144, and possibly at S155 in the case of TRPV6a, may prevent binding either by charge hindrance or by a conformational change.

If phosphorylation of TRPV6 mediates the PMA effect, we should be able to define functionally relevant phosphorylation sites by mutating the consensus site serine or threonine residues. The first site, S144, is solvent exposed (22) (**Fig. 6*A***), and S144A mutants were resistant to rundown in the presence of PMA (Fig. 6*B, C*), confirming the hypothesis that ATP binding may be sterically hindered by phosphorylation at the ARD 3,4 linker region. The faster current development of S144A mutants (+ATP) is partially due to transient expression (see Supplemental Fig. S1). Currents in the absence of ATP were identical to wild type (%REM; Fig. 6*C*).

To test whether other PKC phosphorylation sites are also involved, we mutated single sites detected by the prosite algorithm (35) and investigated the effects of PMA. Figure 6*A* shows the relative location, and Fig. 6*D–F* shows average current densities over time for 3 additional mutants. Three other sites (T150A, S318A, and T702A) showed clear PMA-induced rundown (Fig. 6*D, E, G*). Mutating the dual phosphorylation site T298A/T299A resulted in a weaker effect of PMA, but mutation of the C-terminal site T688A was as efficient as the S144A mutation in blocking the PMA effect (Fig. 6*F, G*). All mutants displayed comparable rundown to wild type in the absence of added ATP (data not shown).We have also confirmed ATP-mediated prevention of rundown for mTRPV5 and for mTRPV6. Although other putative PKC sites are conserved between species, T688 is not a consensus site within mTRPV5, and PMA was unable to oppose the effects of ATP in mTRPV5 (see Supplemental Fig. S2*C–F*). These results point toward a synergistic role of the C-terminal phosphorylation site in mediating the effect of PMA and raise the possibility that a C-terminal region could also be involved in binding of ATP.

Isozyme specificity

To address the specificity of the PMA effect, we incubated TRPV6b cells with an inactive analog of PMA, 4αPDD. This inactive analog was unable to mimic the effects of PMA (**Fig. 7*A***, ***B***), confirming a likely effect on activation of PKCs. We tried to block the effect of PMA by pretreatment with both BIS and Gö6983, inhibitors of classical PKCs, and then added PMA for 1 h. Surprisingly, these inhibitors were unable to prevent the effect of PMA on current

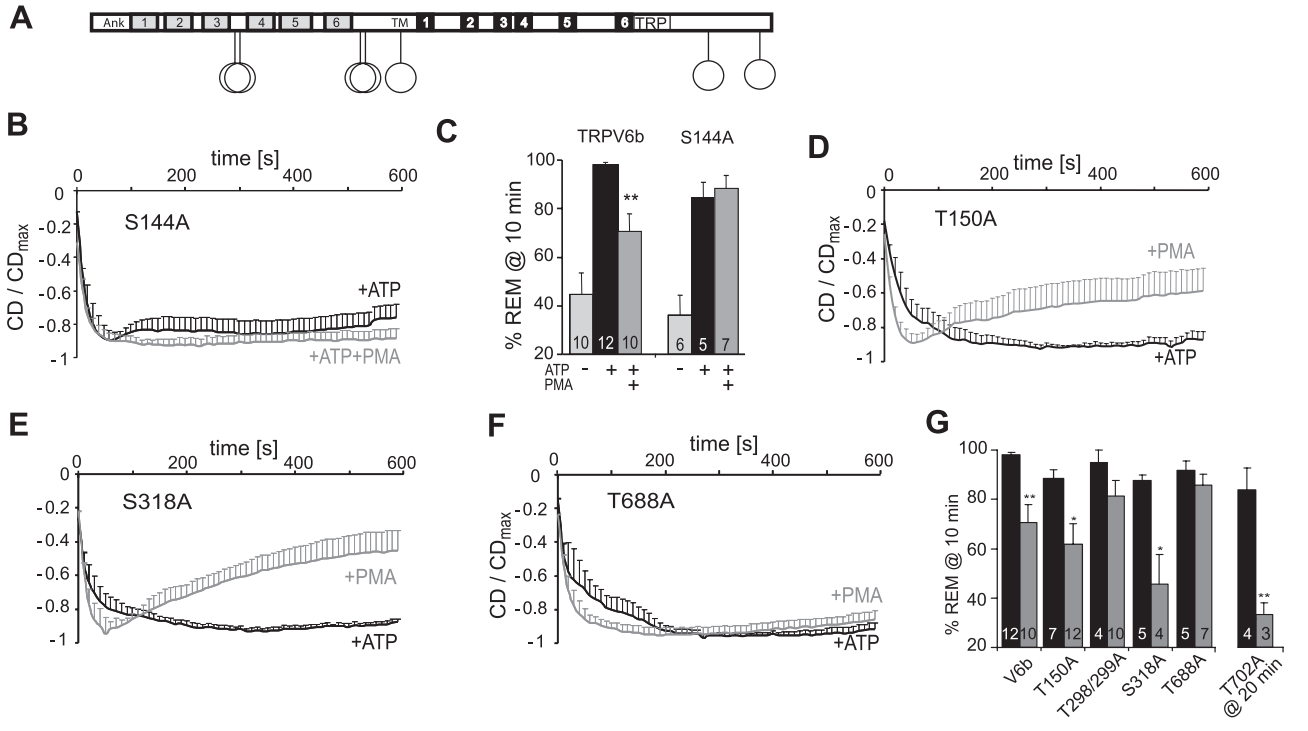

Figure 6. Mutational analysis of PKC phosphorylation sites. *A*) Schematic representation of putative PKC phosphorylation sites as found by the Prosite algorithm. *B*) Normalized current density over time for TRPV6_S144A mutants with and without PMA (500 nM for 1 h) treatment in the presence of ATP. *C*) Quantification of rundown for transiently expressed TRPV6 wild-type and TRPV6 S144A mutants. *D–F*) Normalized current density over time for transiently expressed mutants T150A (*D*), S318A (*E*), and T688A (*F*). *G*) Bar graph showing quantification of rundown in the presence of 3.7 mM free ATP with (gray) or without (black) PMA preincubation.

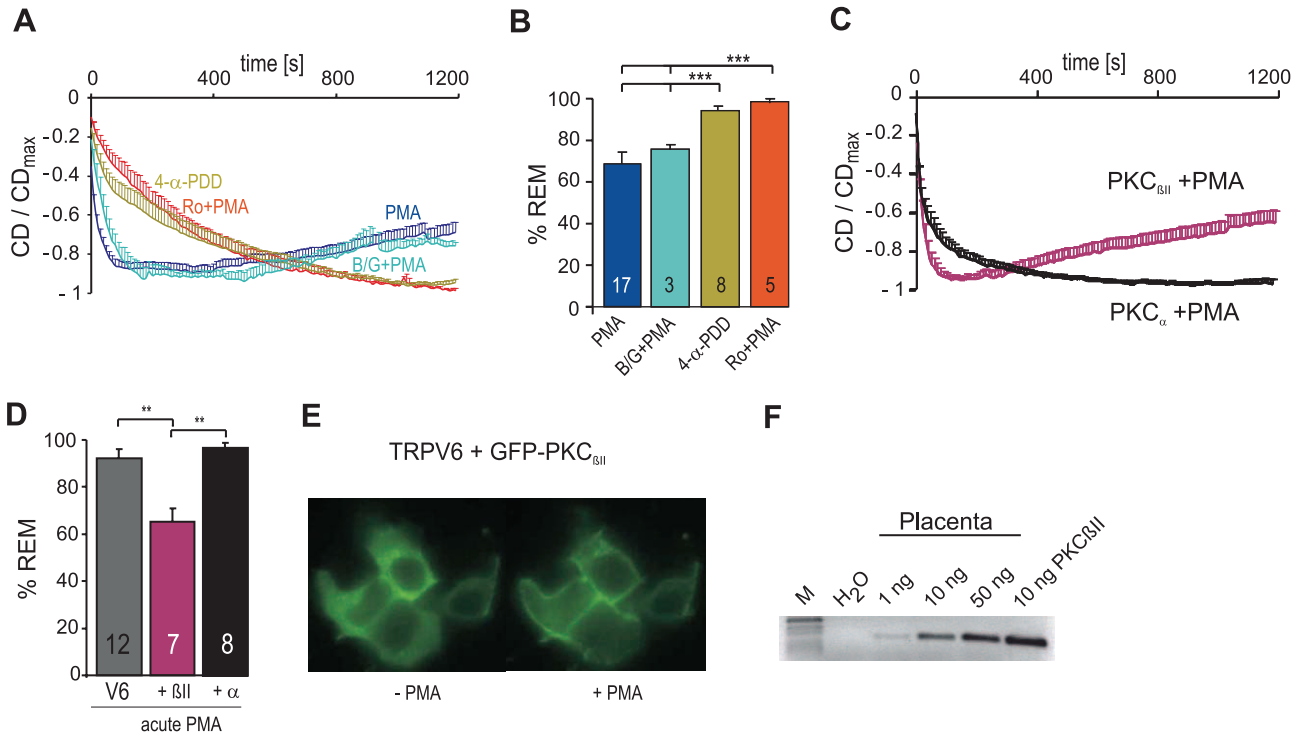

Figure 7. PMA-mediated effects are PKC isoform specific. *A*) Normalized current density over time for TRPV6b-expressing cells that were pretreated either for 1 h with PMA (dark blue) or 4-α-PDD (green) or for 30 min with 500 nM each of inhibitors Gö6983/BIS (light blue) or Ro-31-8220 (orange) and then with inhibitors and 500 nM PMA for 1 h. *B*) Percentage REM for PMA and inhibitors. *C*) Normalized current densities recorded from TRPV6b stable cells with transient expression of GFP-PKC$_{\beta II}$ or GFP-PKC$_{\alpha}$. *D*) Percentage REM with acute (≤10 min in bath) PMA treatment for TRPV6b (V6) cells alone or V6 cells transfected with either GFP-PKC$_{\beta II}$ or GFP-PKC$_{\alpha}$. *A–D*) Internal solution with 3.7 mM free ATP. *E*) Fluorescent images from TRPV6b cells expressing GFP-PKC$_{\beta II}$ before and after PMA-stimulation. *F*) PKC$_{\beta II}$ differs from PKC$_{\beta I}$ by 162 specific C-terminal nucleotides. These were amplified with βII specific primers proportional to the amount of template (human placental cDNA or from recombinant PKC$_{\beta II}$ vector).

development (Fig. 7*A*, *B*). Because neither BIS nor Gö6983 has a defined IC$_{50}$ for the PKC$_{\beta II}$ isoform, we tested whether Ro-31-8322, with an IC$_{50}$ of 14 nM for PKC$_{\beta II}$ (36), was able to prevent PMA from counteracting the ATP effects. Figure 7*A*, *B* shows that Ro-31-8322 was indeed able to suppress the effects of PMA, suggesting that PMA exerts its effects through activation of PKC$_{\beta II}$. Ro-31-8322 alone did not have effects on ATP-modulated TRPV6b currents in the absence of PMA (data not shown). One concern that remained was that long incubation times were necessary to see the effects of PMA, whereas translocation of cPKCs happens within minutes. However, HEK293 cells express only low levels of endogenous PKC$_{\beta II}$ protein (37); therefore, we overexpressed GFP-tagged PKC$_{\beta II}$ or GFP-tagged PKC$_{\alpha}$ and tested whether PMA was now able to exert its effects within minutes. Indeed, with expression of PKC$_{\beta II}$, but not with overexpression of PKC$_{\alpha}$, TRPV6 currents now showed PMA-induced rundown when added to the bath solution without preincubation (Fig. 7*C*, *D*). Both PKC isoforms showed translocation to the plasma membrane after stimulation with PMA (Fig. 7*E* and data not shown). To test if PKC$_{\beta II}$ expression is found in similar tissue types as TRPV6, we checked for its presence in human placenta cDNA (5) using isoform-specific PCR primers and were indeed able to amplify DNA of the correct size (Fig. 7*F*).

ATP binding sites

To screen for additional ATP binding sites, we created fusion proteins (10xHIS at N-term) covering all intracellular protein domains and tested their ability to be retained by ATP-agarose. We found several additional potential binding regions within TRPV6: although the very N-terminal region of the protein containing ARD 1 and 2 (Supplemental Fig. S3*B*) was not retained by ATP-agarose, thus demonstrating that the HIS tag alone does not confer unspecific binding, the ARD region showed weak binding (see also Fig. 5). The N-terminal region between aa 267 and TM1 was also retained (Supplemental Fig. S3*D*). Its sequence contains a basic KKR region as well as a potential PH domain and the dual phosphorylation site T298A/T299A. The proximal region (aa 584-632) of the C-terminal domain containing the TRP motif showed binding that is not efficiently competed for by free ATP, and thus not as specific (Supplemental Fig. S3*E*). However, the distal region (aa 633 to 725; CT) is well retained by ATP-agarose, and binding is effectively

competed for by free ATP (Supplemental Fig. S3*F*). We also checked retention of the ARD region of rat TRPV1 that has been shown to bind ATP (21) (Supplemental Fig. S3*G*). Considering that T688 is a potential phosphorylation site preventing ATP binding (see Fig. 6*F, G* and Supplemental Fig. S2) and the finding that the C-terminal fusion protein encompassing T688 is well retained by ATP-agarose, we wanted to confirm binding to ATP agarose for ARD and CT proteins under native purification conditions. Because proteins containing the N-terminal 10xHIS tag could be solubilized only with urea, we constructed ARD and CT fusion proteins with a C-terminal 6xHIS Tag (Supplemental Fig. S3*H*) and repeated binding experiments after native purification. ARD was retained by ATP-agarose with binding efficiencies of ~10% in several experiments (Coomassie and Western blot), and CT showed binding efficiencies of ~15%, comparable to the proteins purified in the presence of urea. In addition, *in vitro* translated full-length TRPV6 was retained by ATP-agarose in the absence of ATP in the binding buffer, but significantly less in the presence of ATP (data not shown).

Because mutations in individual phosphorylation sites either in the N- or in the C-terminal region (S144, T688) did not show rundown despite PMA incubation and because both fusion proteins encompassing these sites were also retained by ATP-agarose, we suggest a model where ATP directly binds to TRPV6 and might act as a stabilizing factor between the intracellular N and C termini, with residues in both the N- and C-terminal domains necessary for efficient binding in the native protein (see model, **Fig. 8**). The Hill slope of 4.8 as estimated from the dose response (Fig. 3*D*) strengthens this model for a tetrameric channel. Phosphorylation near the N- and C-terminal binding sites destabilizes the protein and tags channels for rundown.

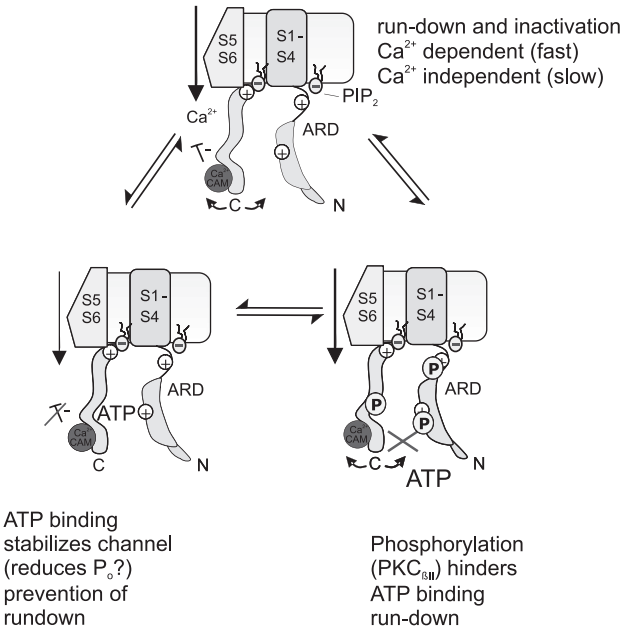

Figure 8. Model of regulatory mechanisms on TRPV6 by ATP and phosphorylation. To simplify graph, only one pore-forming subunit is represented. In the absence of ATP, the channel is prone to both Ca^{2+}-dependent (calmodulin) and Ca^{2+}-independent regulation and rundown. Sufficient ATP stabilizes N and C termini and prevents channel rundown. Phosphorylation hinders ATP binding and thus reduces its stabilizing effect.

DISCUSSION

Stringent regulation of Ca^{2+} influx through TRPV6 is a necessary requirement to avoid Ca^{2+} overload. TRPV6 is inactivated by several Ca^{2+}-dependent pathways such as regulation by calmodulin, breakdown of PIP_2 and probably constitutive exo- and endocytotic mechanisms (38, 39). However, there are also Ca^{2+}-independent mechanisms that lead to channel rundown. Our work identifies ATP as an intracellular ligand that stabilizes the channel and prevents rundown. Because both absolute and normalized maximal current densities are not significantly different within the recording time with or without ATP, ATP does not seem to increase the number of channels in the membrane, although it may prevent the reduction of the number of channels that could lead to rundown. The prevention of rundown does not necessitate hydrolysis of ATP, shows nucleotide specificity (although other phosphorylated nucleotides can partially substitute), and cannot be mimicked by PIP_2. Stabilization of current size shows an EC_{50} of ~380 μM free ATP. This value corresponds well with physiological levels of free ATP and allows the channels to respond to small decreases in ATP concentration to prevent Ca^{2+} overload while the Ca^{2+}-ATPases in the plasma membrane (EC_{50} for ATP 0.1–1 μM; see ref. 40) are still functional. We identified R153 and R154 as being essential for mediating the functional ATP effect. Disruption of this site both by mutagenesis or competition by a peptide resembling this linker sequence disables ATP from decreasing current increments and preventing rundown. Because the RR/QP mutants still show normal currents in the absence of ATP, these mutations did not disturb essential functions not related to the ATP effect. However, charge reversion at this site by creation of RR/EE mutant channels severely reduced current size, which mimics to some extent adding negative charges from ATP's phosphate moieties, but is unable to substitute the adenosine moiety of ATP, which may have its own binding site (see Figs. 3*A, B* and 8). Evidence from ATP-agarose pulldown experiments support a hypothesis that ATP interacts with this N-terminal ARD domain through its negatively charged phosphate groups. Because Phelps *et al.* (22) did not find retention of mTRPV6 ARD by ATP-agarose, we also expressed and purified ARD and CT of hTRPV6 with a similar C-terminal 6xHIS tag under native conditions. ARD still showed binding to ATP-agarose, indicating that species differences or storage conditions (10 mM EDTA, 2.5 mM 2-mercaptoethanol; see ref. 22) may account for differences in binding. The effects of ATP on both current stabilization and activa-

tion kinetics were disrupted when TRPV6 cells (stable or transient expression) were incubated with PMA. This effect is PKC specific and requires activation of $PKC_{\beta II}$, a PKC isoform that is not strongly expressed in HEK293 cells but is present together with TRPV6 in placenta. Overexpression of $PKC_{\beta II}$, but not of $PKC_{\alpha,}$ obliterates the need for PMA preincubation. The results obtained from mutating individual phosphorylation sites argue for a direct effect, where phosphorylation of TRPV6 might hinder binding of ATP. Because both the N-terminal and the distal TRPV6 C-terminal fusion proteins are retained by ATP-agarose and because mutagenesis of putative phosphorylation sites within these domains (S144A and T688A) are able to suppress the PMA effect, we propose a synergistic effect of both binding sites. ATP might form a bridge between both domains and thereby alter channel properties (Fig. 8), leading to slowed current development and reduced rundown. To fully understand the dual effects of ATP, single-channel analyses will be necessary. Low-resolution freeze fracture data obtained for TRPV1 (41) may suggest an interaction between N- and C-terminal regions. Because a mutant that lacks the C-terminal calmodulin binding site of TRPV6 still shows an effect of ATP on rundown (data not shown), the C-terminal ATP binding site does not overlap with the calmodulin binding site, unlike the multiligand binding site of TRPV1 (21).

A small drop in cellular-free ATP levels (*i.e.,* by a 1–2 mM increase in Mg^{2+}; see ref. 42) leads to channels less stable and more prone to both Ca^{2+}-dependent and Ca^{2+}-independent rundown phenomena and thus a reduction in overall Ca^{2+} influx. Activation of $PKC_{\beta II}$ prevents stabilization by ATP, and channels show more rundown and Ca^{2+}-dependent inactivation. The upstream GPCR that activates $PKC_{\beta II}$ *in vivo* may thus be involved in feedback regulation when sufficient Ca^{2+} has been taken up by TRPV6 and may also be responsible for conferring an allele-specific advantage. It will be interesting to analyze if and how both kinases regulate the native channels. Unfortunately, these studies are hampered by the difficulty in obtaining human cells in which native TRPV6 currents can be measured. FJ

We especially thank Dr. Veit Flockerzi and Dr. Ulrich Wissenbach (University of Saarland, Homburg, Germany) for the stable TRPV6 cell lines, for antibodies against TRPV6 and the HIS tag, and, together with Dr. Hoth, for discussions and critical reading of the manuscript. We also thank Dr. Yusuf Hannun (Medical University of South Carolina, Charleston, SC, USA) and Dr. Peter Lipp (University of Saarland) for kindly providing us with the cDNA for $GFP\text{-}PKC_{\beta II}$ and $GFP\text{-}PKC_{\alpha}$; Dr. Marcel Meissner (University of Saarland) for fusion proteins of mTRPV6; Heidi Löhr, Anja Ludes, and Bettina Strauß for cell culture work; and members of the labs for critical input. This work was supported, in part, by the Deutsche Forschungsgemeinschaft (DFG; NI 671 to B.N.) and HOMFOR (B.N.). D.A.-A. is a member of the DFG-sponsored graduate program GK 1326.

REFERENCES

1. Suzuki, Y., Landowski, C. P., and Hediger, M. A. (2008) Mechanisms and regulation of epithelial Ca2+ absorption in health and disease. *Annu. Rev. Physiol.* **70,** 257–271
2. Van de Graaf, S. F., Bindels, R. J., and Hoenderop, J. G. (2007) Physiology of epithelial Ca2+ and Mg2+ transport. *Rev. Physiol. Biochem. Pharmacol.* **158,** 77–160
3. Nilius, B., Vennekens, R., Prenen, J., Hoenderop, J. G., Bindels, R. J., and Droogmans, G. (2000) Whole-cell and single channel monovalent cation currents through the novel rabbit epithelial Ca2+ channel ECaC. *J. Physiol.* **527**(Pt. 2), 239–248
4. Vennekens, R., Hoenderop, J. G., Prenen, J., Stuiver, M., Willems, P. H., Droogmans, G., Nilius, B., and Bindels, R. J. (2000) Permeation and gating properties of the novel epithelial Ca(2+) channel. *J. Biol. Chem.* **275,** 3963–3969
5. Wissenbach, U., Niemeyer, B. A., Fixemer, T., Schneidewind, A., Trost, C., Cavalie, A., Reus, K., Meese, E., Bonkhoff, H., and Flockerzi, V. (2001) Expression of CaT-like, a novel calcium-selective channel, correlates with the malignancy of prostate cancer. *J. Biol. Chem.* **276,** 19461–19468
6. Nilius, B., Prenen, J., Vennekens, R., Hoenderop, J. G., Bindels, R. J., and Droogmans, G. (2001) Modulation of the epithelial calcium channel, ECaC, by intracellular Ca2+. *Cell Calcium* **29,** 417–428
7. Bodding, M., Wissenbach, U., and Flockerzi, V. (2002) The recombinant human TRPV6 channel functions as Ca2+ sensor in human embryonic kidney and rat basophilic leukemia cells. *J. Biol. Chem.* **277,** 36656–36664
8. Nilius, B., Prenen, J., Hoenderop, J. G., Vennekens, R., Hoefs, S., Weidema, A. F., Droogmans, G., and Bindels, R. J. (2002) Fast and slow inactivation kinetics of the Ca2+ channels ECaC1 and ECaC2 (TRPV5 and TRPV6): role of the intracellular loop located between transmembrane segments 2 and 3. *J. Biol. Chem.* **277,** 30852–30858
9. Hoenderop, J. G., Voets, T., Hoefs, S., Weidema, F., Prenen, J., Nilius, B., and Bindels, R. J. (2003) Homo- and heterotetrameric architecture of the epithelial Ca2+ channels TRPV5 and TRPV6. *EMBO J.* **22,** 776–785
10. Niemeyer, B. A., Bergs, C., Wissenbach, U., Flockerzi, V., and Trost, C. (2001) Competitive regulation of CaT-like-mediated Ca2+ entry by protein kinase C and calmodulin. *Proc. Natl. Acad. Sci. U. S. A.* **98,** 3600–3605
11. Derler, I., Hofbauer, M., Kahr, H., Fritsch, R., Muik, M., Kepplinger, K., Hack, M. E., Moritz, S., Schindl, R., Groschner, K., and Romanin, C. (2006) Dynamic but not constitutive association of calmodulin with rat TRPV6 channels enables fine tuning of Ca2+-dependent inactivation. *J. Physiol.* **577,** 31–44
12. Thyagarajan, B., Lukacs, V., and Rohacs, T. (2008) Hydrolysis of phosphatidylinositol 4,5-bisphosphate mediates calcium-induced inactivation of TRPV6 channels. *J. Biol. Chem.* **283,** 14980–14987
13. Lee, J., Cha, S. K., Sun, T. J., and Huang, C. L. (2005) PIP2 activates TRPV5 and releases its inhibition by intracellular Mg2+. *J. Gen. Physiol.* **126,** 439–451
14. Hilgemann, D. W. (1997) Cytoplasmic ATP-dependent regulation of ion transporters and channels: mechanisms and messengers. *Annu. Rev. Physiol.* **59,** 193–220
15. Craig, T. J., Ashcroft, F. M., and Proks, P. (2008) How ATP inhibits the open K(ATP) channel. *J. Gen. Physiol.* **132,** 131–144
16. Dhar-Chowdhury, P., Malester, B., Rajacic, P., and Coetzee, W. A. (2007) The regulation of ion channels and transporters by glycolytically derived ATP. *Cell. Mol. Life Sci.* **64,** 3069–3083
17. Takahashi, M., Kondou, Y., and Toyoshima, C. (2007) Interdomain communication in calcium pump as revealed in the crystal structures with transmembrane inhibitors. *Proc. Natl. Acad. Sci. U. S. A.* **104,** 5800–5805
18. Kameyama, M., Kameyama, A., Takano, E., and Maki, M. (1998) Run-down of the cardiac L-type Ca2+ channel: partial restoration of channel activity in cell-free patches by calpastatin. *Pflügers Arch.* **435,** 344–349
19. Romanin, C., Grosswagen, P., and Schindler, H. (1991) Calpastatin and nucleotides stabilize cardiac calcium channel activity in excised patches. *Pflügers Arch.* **418,** 86–92
20. Okashiro, T., Tokuno, H., Fukumitsu, T., Hayashi, H., and Tomita, T. (1992) Effects of intracellular ATP on calcium

current in freshly dispersed single cells of guinea-pig portal vein. *Exp. Physiol.* **77,** 719–731
21. Lishko, P. V., Procko, E., Jin, X., Phelps, C. B., and Gaudet, R. (2007) The ankyrin repeats of TRPV1 bind multiple ligands and modulate channel sensitivity. *Neuron* **54,** 905–918
22. Phelps, C. B., Huang, R. J., Lishko, P. V., Wang, R. R., and Gaudet, R. (2008) Structural analyses of the ankyrin repeat domain of TRPV6 and related TRPV ion channels. *Biochemistry* **47,** 2476–2484
23. Akey, J. M., Swanson, W. J., Madeoy, J., Eberle, M., and Shriver, M. D. (2006) TRPV6 exhibits unusual patterns of polymorphism and divergence in worldwide populations. *Hum. Mol. Genet.* **15,** 2106–2113
24. Hughes, D. A., Tang, K., Strotmann, R., Schoneberg, T., Prenen, J., Nilius, B., and Stoneking, M. (2008) Parallel selection on TRPV6 in human populations. *PLoS ONE* **3,** e1686
25. Fixemer, T., Wissenbach, U., Flockerzi, V., and Bonkhoff, H. (2003) Expression of the Ca2+-selective cation channel TRPV6 in human prostate cancer: a novel prognostic marker for tumor progression. *Oncogene* **22,** 7858–7861
26. Abdalla, I., Ray, P., Ray, V., Vaida, F., and Vijayakumar, S. (1998) Comparison of serum prostate-specific antigen levels and PSA density in African-American, white, and Hispanic men without prostate cancer. *Urology* **51,** 300–305
27. Grynkiewicz, G., Poenie, M., and Tsien, R. Y. (1985) A new generation of Ca2+ indicators with greatly improved fluorescence properties. *J. Biol. Chem.* **260,** 3440–3450
28. Jin, X., Touhey, J., and Gaudet, R. (2006) Structure of the N-terminal ankyrin repeat domain of the TRPV2 ion channel. *J. Biol. Chem.* **281,** 25006–25010
29. Voets, T., Janssens, A., Prenen, J., Droogmans, G., and Nilius, B. (2003) Mg(2+)-dependent gating and strong inward rectification of the cation channel TRPV6. *J. Gen. Physiol.* **121,** 245–260
30. Hoenderop, J. G., Vennekens, R., Muller, D., Prenen, J., Droogmans, G., Bindels, R. J., and Nilius, B. (2001) Function and expression of the epithelial Ca(2+) channel family: comparison of mammalian ECaC1 and 2. *J. Physiol.* **537,** 747–761
31. Zhang, X. D., Tseng, P. Y., and Chen, T. Y. (2008) ATP inhibition of CLC-1 is controlled by oxidation and reduction. *J. Gen. Physiol.* **132,** 421–428
32. Schwoebel, E. D., Ho, T. H., and Moore, M. S. (2002) The mechanism of inhibition of Ran-dependent nuclear transport by cellular ATP depletion. *J. Cell Biol.* **157,** 963–974
33. Guerini, D., Coletto, L., and Carafoli, E. (2005) Exporting calcium from cells. *Cell Calcium* **38,** 281–289
34. Rohacs, T., Lopes, C. M., Michailidis, I., and Logothetis, D. E. (2005) PI(4,5)P2 regulates the activation and desensitization of TRPM8 channels through the TRP domain. *Nat. Neurosci.* **8,** 626–634
35. Combet, C., Blanchet, C., Geourjon, C., and Deleage, G. (2000) NPS@: network protein sequence analysis. *Trends Biochem. Sci.* **25,** 147–150
36. Wilkinson, S. E., Parker, P. J., and Nixon, J. S. (1993) Isoenzyme specificity of bisindolylmaleimides, selective inhibitors of protein kinase C. *Biochem. J.* **294**(Pt. 2), 335–337
37. Feng, X., Zhang, J., Barak, L. S., Meyer, T., Caron, M. G., and Hannun, Y. A. (1998) Visualization of dynamic trafficking of a protein kinase C betaII/green fluorescent protein conjugate reveals differences in G protein-coupled receptor activation and desensitization. *J. Biol. Chem.* **273,** 10755–10762
38. Cha, S. K., Wu, T., and Huang, C. L. (2008) Protein kinase C inhibits caveolae-mediated endocytosis of TRPV5. *Am. J. Physiol. Renal Physiol.* **294,** F1212–F1221
39. Van de Graaf, S. F., Rescher, U., Hoenderop, J. G., Verkaart, S., Bindels, R. J., and Gerke, V. (2008) TRPV5 is internalized via clathrin-dependent endocytosis to enter a Ca2+-controlled recycling pathway. *J. Biol. Chem.* **283,** 4077–4086
40. Guerini, D. (1998) The significance of the isoforms of plasma membrane calcium ATPase. *Cell Tissue Res.* **292,** 191–197
41. Moiseenkova-Bell, V. Y., Stanciu, L. A., Serysheva, I. I., Tobe, B. J., and Wensel, T. G. (2008) Structure of TRPV1 channel revealed by electron cryomicroscopy. *Proc. Natl. Acad. Sci. U. S. A.* **105,** 7451–7455
42. Romani, A. M., and Scarpa, A. (2000) Regulation of cellular magnesium. *Front. Biosci.* **5,** D720–D734

Received for publication July 14, 2009.
Accepted for publication September 10, 2009.